Geophysical Research Letters

RESEARCH LETTER
10.1029/2024GL111902

A Factor Two Difference in 21st-Century Greenland Ice Sheet Surface Mass Balance Projections From Three Regional Climate Models Under a Strong Warming Scenario (SSP5-8.5)

Q. Glaude[1,2], B. Noel[1], M. Olesen[3], M. Van den Broeke[4], W. J. van de Berg[4], R. Mottram[3], N. Hansen[3], A. Delhasse[1,5], C. Amory[6], C. Kittel[1,6], H. Goelzer[7], and X. Fettweis[1]

[1]Laboratory of Climatology, University of Liège, Liège, Belgium, [2]Applied Computer Electronics Laboratory, University of Liège, Liège, Belgium, [3]Danish Meteorological Institute (DMI), Copenhagen, Denmark, [4]Institute for Marine and Atmospheric Research (IMAU), Utrecht University, Utrecht, The Netherlands, [5]Earth and Life Institute, Université Catholique de Louvain, Louvain-la-Neuve, Belgium, [6]Institut des Géosciences de l'Environnement (IGE), Université Grenoble Alpes/CNRS/IRD/G-INP, Grenoble, France, [7]NORCE Norwegian Research Centre, Bjerknes Centre for Climate Research, Bergen, Norway

Abstract The Arctic is warming rapidly, significantly reducing the Greenland ice sheet (GrIS) surface mass balance (SMB) and raising its contribution to global sea-level rise. Since these trends are expected to continue, it is essential to explore the GrIS SMB response to projected climate warming. We compare projections from three polar regional climate models, RACMO, MAR, and HIRHAM, forced by the Community Earth System Model CESM2 under a high-end warming scenario (SSP5-8.5, 1970–2099). We reveal different modeled SMB by 2100, including a twofold larger annual surface mass loss in MAR (−1735 Gt/yr) and HIRHAM (−1698 Gt/yr) relative to RACMO (−964 Gt/yr). Discrepancies primarily stem from differences in projected runoff, triggering melt-albedo positive feedback and subsequent modeled ablation zone expansion. In addition, we find different responses of modeled meltwater production to similar atmospheric warming. Our analysis suggests clear avenues for model developments to further improve SMB projections and contribution to sea-level rise.

Plain Language Summary We explore how three different polar climate models predict the future surface mass balance (SMB) of the Greenland ice sheet (GrIS), a major contributor to global sea-level rise. Our results show that SMB projections among these models differ significantly by the end of the century. Differences primarily stem from how models convert meltwater into surface runoff toward the ocean, a crucial SMB component that directly contributes to sea-level rise. Another key factor is the response of these models to climate warming, substantially affecting future melting rates. Our research highlights the need for further improvements of these climate models. By identifying and understanding the drivers behind model differences, we can improve SMB predictions and better estimate future global sea-level rise.

Key Points:

- With identical forcing, Greenland Ice Sheet surface mass balance from 3 regional climate models shows a two-fold difference by 2100
- Different runoff projections stem from substantial discrepancies in projected ablation zone expansion, and reciprocally
- The response of meltwater production to similar atmospheric warming differs significantly among regional climate models

Supporting Information:

Supporting Information may be found in the online version of this article.

Correspondence to:

Q. Glaude,
quentin.glaude@uliege.be

Citation:

Glaude, Q., Noel, B., Olesen, M., Van den Broeke, M., van de Berg, W. J., Mottram, R., et al. (2024). A factor two difference in 21st-century Greenland ice sheet surface mass balance projections from three regional climate models under a strong warming scenario (SSP5-8.5). *Geophysical Research Letters*, *51*, e2024GL111902. https://doi.org/10.1029/2024GL111902

Received 21 AUG 2024
Accepted 31 OCT 2024

Author Contributions:

Conceptualization: B. Noel, M. Olesen, C. Amory, C. Kittel, X. Fettweis
Data curation: Q. Glaude
Formal analysis: Q. Glaude, M. Van den Broeke, C. Kittel
Funding acquisition: X. Fettweis
Investigation: Q. Glaude, B. Noel, M. Van den Broeke, A. Delhasse, C. Amory, C. Kittel
Methodology: Q. Glaude, B. Noel, C. Amory, C. Kittel, X. Fettweis
Project administration: X. Fettweis
Resources: M. Olesen, X. Fettweis

1. Introduction

Mass loss of the Greenland ice sheet (GrIS) currently contributes 25% (or 0.6 mm/yr, 2013–2017) to global mean sea-level rise (SLR) (Goelzer et al., 2020; IMBIE, 2019). Completely melted, the GrIS would raise global sea-level by over 7 m (Morlighem et al., 2017). Decreased GrIS Surface Mass Balance (SMB) contributes about 50% of mass loss (IMBIE, 2019), a rate that is projected to increase in the future (Nowicki et al., 2016). Under high greenhouse gas emissions pathways (SSP5-8.5), projections estimate a SLR of up to 1 m by 2100 (IPCC, 2023), with the current imbalance already implies a 27 cm SLR from the GrIS (Box et al., 2022).

GrIS mass loss is about equally distributed between increased solid ice discharge from calving icebergs, and increased surface mass loss from runoff (Goelzer et al., 2020). GrIS SMB, that is, the difference between surface accumulation from snowfall and ablation from runoff, has significantly decreased in recent decades (Noël et al., 2021). Warm summers in 2012 and 2019 have triggered record melt events at the highest altitudes of the GrIS (Hanna et al., 2021; Tedesco et al., 2020). The associated enhanced runoff has contributed to increase ice mass loss in Greenland (Bevis et al., 2019). The regional response of surface melt to atmospheric warming, such as variations in surface albedo in southwestern Greenland, introduces challenges in projecting GrIS SMB and

Supervision: B. Noel, M. Van den Broeke, C. Kittel, X. Fettweis
Validation: Q. Glaude, M. Van den Broeke
Visualization: Q. Glaude
Writing – original draft: Q. Glaude
Writing – review & editing: Q. Glaude, B. Noel, M. Olesen, M. Van den Broeke, A. Delhasse, C. Amory, C. Kittel, H. Goelzer, X. Fettweis

future SLR contributions (Bevis et al., 2019), which are further compounded by the disproportionate effects of short-term atmospheric variability on ice-sheet SMB (Hanna et al., 2024).

In this context, the Ice Sheet Model Intercomparison Project aims at improving future SLR contributions from the Greenland and Antarctic ice sheets using an ensemble of ice sheet model mass loss projections. The last iteration, ISMIP6 (Nowicki et al., 2016), produced projections of Greenland's contribution to SLR based on SMB downscaling of only one polar Regional Climate Model (RCM), namely MAR (Goelzer et al., 2020). Various studies employing RCMs such as MAR, RACMO, and HIRHAM have been conducted separately to explore Greenland's future climate scenarios (Hofer et al., 2020; Mottram et al., 2017; Noël et al., 2021, 2022), examining the sensitivity of these models to different emission scenarios and forcings from large-scale Earth System Models (ESMs), and highlighting the significant discrepancies in GrIS SMB projections arising from the climate forcing itself.

The GrSMBMIP intercomparison exercise conducted by Fettweis et al. (2020), ensuring consistency in data forcing and output grid, found a general agreement on contemporary SMB estimates (1980–2012) among the models MAR, RACMO, and HIRHAM, using reanalysis data. Following the same approach, we compare the three RCMs used to dynamically downscale climate projections from CESM2 under a high-end warming scenario (SSP5-8.5) until 2,100. Through this comparison exercise, we aim at highlighting model differences and suggest improvements to refine future SLR projections.

2. Data and Methods

2.1. Polar-Oriented Regional Climate Models

Polar RCMs forced by ESMs dynamically downscale atmospheric conditions to finer resolution, by incorporating more detailed or regionally relevant physics. In this study, we use CESM2 (Danabasoglu et al., 2020), a model developed by the National Center for Atmospheric Research (NCAR), part of the Coupled Model Intercomparison Project (CMIP), Phase 6. CESM2 is one of the first CIMP6 ESMs to provide 6-hourly forcing data, required for RCMs. CESM2 integrates various components of the Earth's climate system including the atmosphere, oceans, land ice and sea ice, and their interactions on a nominal 1° horizontal resolution (Gettelman et al., 2019). The model was run for the period 1970–2100 under the high emission Shared Socio-Economic Pathways (SSP5-8.5), that is, with an additional radiative forcing of 8.5 W/m^2 by the year 2100 compared to the pre-industrial period. SSP5-8.5 was selected to explore model sensitivity to extreme warming conditions. The forcing data of the three RCMs include temperature, specific humidity, pressure, wind speed, and direction, prescribed at the lateral boundaries for each of the vertical atmospheric hybrid levels of the RCMs. Sea Surface Temperature (SST) and Sea Ice Concentration (SIC) from CESM2 are also prescribed for the three RCMs. These RCMs have a fixed ice sheet geometry, excluding melt-elevation feedback and the impact of topography changes on atmospheric circulation and precipitation. Noël et al. (2020) and van Kampenhout et al. (2020) shows that RACMO-CESM2 yields realistic SMB in the historical period 1950–2014 compared to ERA-forced RACMO, GRACE, and in situ SMB observations.

2.1.1. RACMO

The Regional Atmospheric Climate Model - RACMO 2.3p2 is a regional climate model for future applications over the GrIS run at 11 km horizontal resolution (Noël et al., 2020, 2021, 2022). RACMO integrates the dynamical core of the High-Resolution Limited Area Model (HIRLAM) and the physics package from the ECMWF Integrated Forecast System (ECMWF-IFS), cY33r1. RACMO includes 40 active snow layers that are initialized using estimates of temperature and density profiles derived from the IMAU Firn Densification Model (IMAU-FDM) (Ligtenberg et al., 2011). These profiles are obtained by repeatedly running IMAU-FDM over 1960–1980 until the full firn layer is refreshed. RACMO also includes a snow module simulating melt, retention, refreezing, and runoff (Ettema et al., 2010). In the present version, snow albedo is simulated based on snow impurities, zenith angle, and metamorphism (Kuipers Munneke, 2011). Baer ice albedo is derived from a MODIS albedo product, estimated as the 5% lowest values measured annually, averaged over 2000–2015. The model uses topography from the GIMP DEM (Howat et al., 2014) at 90 m, down-sampled to 11 km. Further resampling of RACMO outputs to the ISMIP6 1-km common grid follows a statistical downscaling approach that includes elevation bias correction of SMB estimates (Noel et al., 2016). Additional setup details for RACMO and other RCMs are provided in Supporting Information S1 (Table S1).

2.1.2. MAR

The Modèle Atmosphérique Régional - MARv3.12 (Hofer et al., 2020; Lambin et al., 2023) is a RCM widely used in polar research, here run at a horizontal resolution of 15 km. It is built on the hydrostatic approximation of the primitive equations (Gallée & Schayes, 1994) and incorporates a microphysics module from Gallee, 1995. The model includes a radiative transfer scheme akin to the ECMWF ERA-40 reanalysis (Morcrette, 2002) and the SISVAT (Soil Ice Snow Vegetation Atmosphere Transfer) module, modeling water mass and energy exchanges between the atmosphere and the surface (De Ridder & Gallée, 1998). The model also includes a detailed snow module based on the CROCUS model (Brun et al., 1992; Lefebre et al., 2005), representing 30 layers of snow metamorphism, with variable vertical depth. MAR dynamically calculates surface albedo, adjusting for snow properties and cloud presence (Tedesco et al., 2016). Over baer ice, MAR albedo remains constant at 0.55 across the GrIS ablation zone (with slight variation due to temporal snow). MAR utilizes the ArcticDEM data product (Porter et al., 2018) for base topography. The resampling to the 1-km common grid utilizes topographic corrections of SMB biases (Franco et al., 2012).

2.1.3. HIRHAM

HIRHAM5 (contraction of HIRLAM and ECHAM models) is a hydrostatic RCM specifically optimized to represent ice sheet surface processes at high resolution of 5 km (Christensen et al., 2007; Mottram et al., 2017). It is developed based on the physics scheme of the ECMWF Hamburg Atmospheric Model - ECHAM5 global climate model (Roeckner et al., 2003) and the numerical weather forecast model HIRLAM7 (Eerola, 2006). The outputs from HIRHAM5 are used to force an offline subsurface model, based on ECHAM5 physics (Roeckner et al., 2003) incorporating updates to an advanced albedo scheme. HIRHAM5 includes 32 dynamic subsurface snow layers, updated through processes such as snowfall, melt, retention of liquid water, refreezing, runoff, sublimation, and rain (Langen et al., 2015). Consequently, the subsurface model is driven by inputs of snowfall, rainfall, evaporation, sublimation, and surface energy fluxes from HIRHAM5. Following the approach outlined by Langen et al. (2015), the shortwave albedo is internally computed, employing snow albedo ranging from 0.85 below −5°C to 0.65 at 0°C for the upper-level temperature. The albedo for baer ice remains constant at 0.4. Additionally, a transition albedo is determined for thin snow layers on ice, utilizing the method proposed by Oerlemans and Knap (1998). HIRHAM uses the DEM from Bamber et al. (2001) for base topography, utilized for resampling HIRHAM products to the 1-km common grid.

2.2. Methodology

GrIS mass change is closely linked to its SMB, defined as the net balance at the surface between mass gains from precipitation and losses mainly due to runoff. Despite their minor contribution, SMB calculation also accounts for sublimation, deposition, and drifting snow erosion:

$$\mathrm{SMB} = \mathrm{RF} + \mathrm{SF} - \mathrm{RU} - \mathrm{SU} + \mathrm{DE} \quad (1)$$

In this equation, Rainfall (RF) and Snowfall (SF) represent liquid and solid precipitation terms, respectively. Runoff (RU) is the liquid water flowing toward the ocean, Sublimation (SU) is the phase transition from ice to vapor, and Deposition (DE) refers to the net accumulation of airborne particles minus erosion. Runoff is estimated within each model snow module as:

$$\mathrm{Runoff} = \mathrm{Melt} + \mathrm{Condensation} - \mathrm{Retention} - \mathrm{Refreeze} \quad (2)$$

The first two terms account for the liquid water filling the snowpack pore space. The last two terms account for the water maintained within the porous regions of the snow by capillary forces, while refreezing represents the transition from liquid water to solid water. In these numerical models, the vertical transport of meltwater in the snowpack follows a bucket model: a saturated gridcell transfers the water downwards (percolation), filling the underlying gridcell. Excess water in the bottom layer is converted into runoff. The presence of ice lenses in intermediary layers can modify the percolation scheme (MAR partially converts meltwater to runoff, while RACMO does not—see Table S1 in Supporting Information S1). The maximum snowpack retention capacity retained by capillarity is parametrized by the irreducible water saturation index (IWS), that typically ranges from

2% to 15% across the ice sheet (Coléou & Lesaffre, 1998). Melt production is driven by the ice sheet surface energy balance (SEB) as:

$$SEB = SWD + SWU + LWD + LWU + SHF + LHF + GHF \quad (3)$$

With SWD and SWU being the shortwave downwards and upwards radiations, LWD and LWU the longwave downwards and upwards radiations, SHF the sensible heat flux, LHF the latent heat flux, and GHF the conductive ground heat flux from underground layers to the surface snow layers. A positive sign represents energy added to the surface.

To ensure a meaningful comparison, major model outputs are reprojected onto a common 1 km grid based on the ISMIP6 effort (Goelzer et al., 2020), including peripheral glaciers and ice caps. The resampling of RCM outputs follows model-specific topographic corrections of SMB components: Noël et al. (2016) for RACMO outputs, Franco et al. (2012) for MAR and HIRHAM outputs.

3. Results, or a Descriptive Heading About the Results

Figure 1 presents the GrIS SMB for the period 2080–2099 (Figures 1a–1c) and anomalies (Figures 1d–1f) as modeled by RACMO, MAR, and HIRHAM, respectively. In this section, anomalies are always computed with respect to 1980–1999.

Although forced by the same 6-hourly input from CESM2, we find large discrepancies between models by 2080–2099. SMB in RACMO (Figure 1a) is generally higher than in MAR (Figure 1b) and HIRHAM (Figure 1c), with a larger inland accumulation (SMB >0) zone and subsequently smaller ablation zone (SMB <0). In the period 2080–2099, the fraction of the ice sheet being in the ablation zone significantly differs between the three models, with 47% in RACMO, 70% in MAR, and 87% in HIRHAM. Unlike RACMO and MAR, HIRHAM shows almost no accumulation zone by the end of the century (Figure 1c).

The SMB anomaly maps (Figures 1d–1f) reveal substantial reductions in SMB, particularly around the periphery of the ice sheet. The pattern of these anomalies varies significantly between models. While all models show a progressive increase in the magnitude of SMB anomalies toward the GrIS margins, the transition is steeper for MAR and HIRHAM compared to RACMO, notably toward the southeastern and western margins where anomalies can exceed 10 m water equivalent (WE) per year.

Figure 2 represents modeled SMB component anomalies, including SMB (Figure 2a), total precipitation (snowfall and rainfall, PP, Figure 2b), and runoff (RU, Figure 2c) for the period 1970–2099 for the three models. For further details, Figures S1 and S2 in Supporting Information S1 show SMB and runoff projections for the period 1970–2100 for six Greenland basins as utilized in Fettweis et al., 2020.

SMB anomalies indicate a decline in all three models toward the end of the century (Figure 2a). By 2099, RACMO, MAR, and HIRHAM project SMB anomalies of −1,331 Gt/yr, −2,105 Gt/yr, and −1,895 Gt/yr, respectively, highlighting pronounced model variability. Notably, MAR shows the largest SMB decline. The increasingly negative SMB values toward the end of the century reflect the accelerating rate of mass loss.

Figure 2b illustrates precipitation anomalies, indicating increasing precipitation over time. By 2100, all models simulate precipitation anomalies of approximately 200–250 Gt/year, indicating a similar trend among the models.

Runoff anomalies significantly increase by the end of the century (Figure 2c), reaching 1,560 Gt/year for RACMO, 2,313 Gt/year for MAR, and 2,144 Gt/year for HIRHAM. The precipitation increase is insufficient to counterbalance the enhanced surface mass loss from runoff. The relatively small increase in precipitation anomalies suggest that changes in precipitation have a marginal effect on SMB anomalies, which are dominated by a significant increase in runoff.

Figure 3 illustrates the ratio of meltwater that runs off to the ocean by the end of the century (2080–2099) for the RACMO, MAR, and HIRHAM models.

In the ablation zone (Figure 3), meltwater production approximately equals runoff, assuming that rainfall has a lower magnitude contribution to the total liquid water content. Figure 3 is a clear indicator of the refreezing fraction, that is, the fraction of total liquid water content that does not run off. It also highlights differences in the

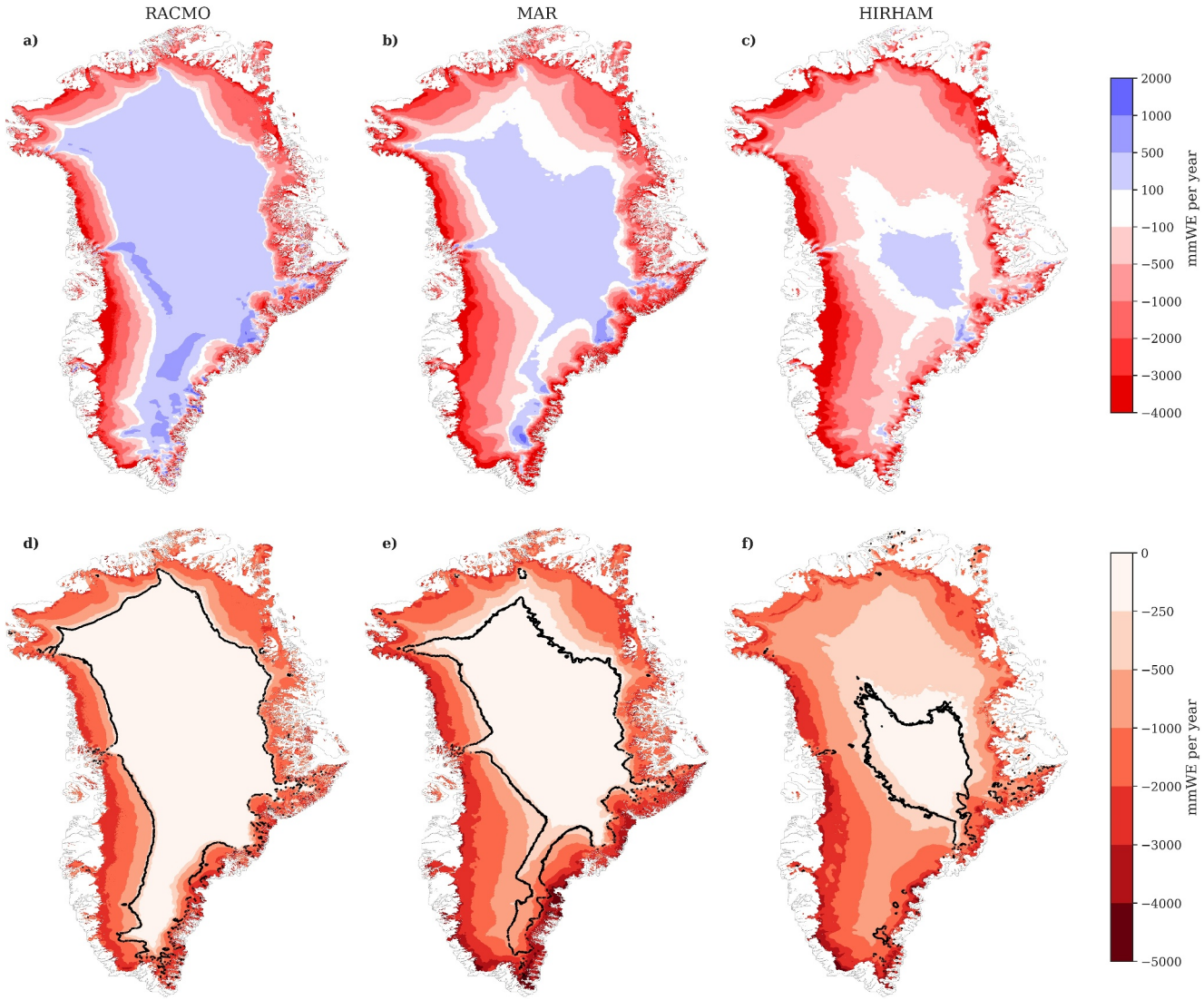

Figure 1. GrIS annual surface mass balance (a, b, c, 2080–2099 average) and annual surface mass balance anomaly (d, e, f, 2080–2099 average relative to 1980–1999) [mm WE/yr]. From left to right, RACMO (a and d), MAR (b and e), and HIRHAM (c and f). The equilibrium line (SMB = 0) is displayed as a solid black line in (d-f).

firn models used by each climate model, including porosity, retention capacities, and saturation levels, as discussed later.

Figure 4 illustrates the sensitivity of modeled surface melt (Figure 4a), liquid precipitation (Figure 4b), and runoff (Figure 4c) to 2-m temperature anomalies. Meltwater is by far the primary contributor to the total liquid water content within the snowpack, driving runoff and mass loss of the GrIS (Figure 4a). The models have different sensitivities to temperature anomalies. At lower temperatures, RACMO produces more melt, but as temperature anomalies rise, MAR and HIRHAM generate significantly more meltwater. At +8°C anomalies, the differences between the models become more pronounced, with MAR producing up to 25% more meltwater, eventually contributing to significant runoff fluxes (2,889 Gt/yr for 2090–2099, compared to 2,323 Gt/yr for RACMO). Figure 4b shows that liquid precipitation (rainfall) increases linearly with temperature anomalies, but the absolute variations between models are negligible compared to meltwater production.

To explain the large melt differences among models, Figure S3 (Supporting Information S1) shows the evolution of major surface energy balance components (Equation 3) for the Greenland ice sheet during summer months (June-July-August) from 1970 to 2100. By the end of the century, MAR surface energy balance is 8 W/m^2 higher on average than RACMO, explaining the higher meltwater production in MAR.

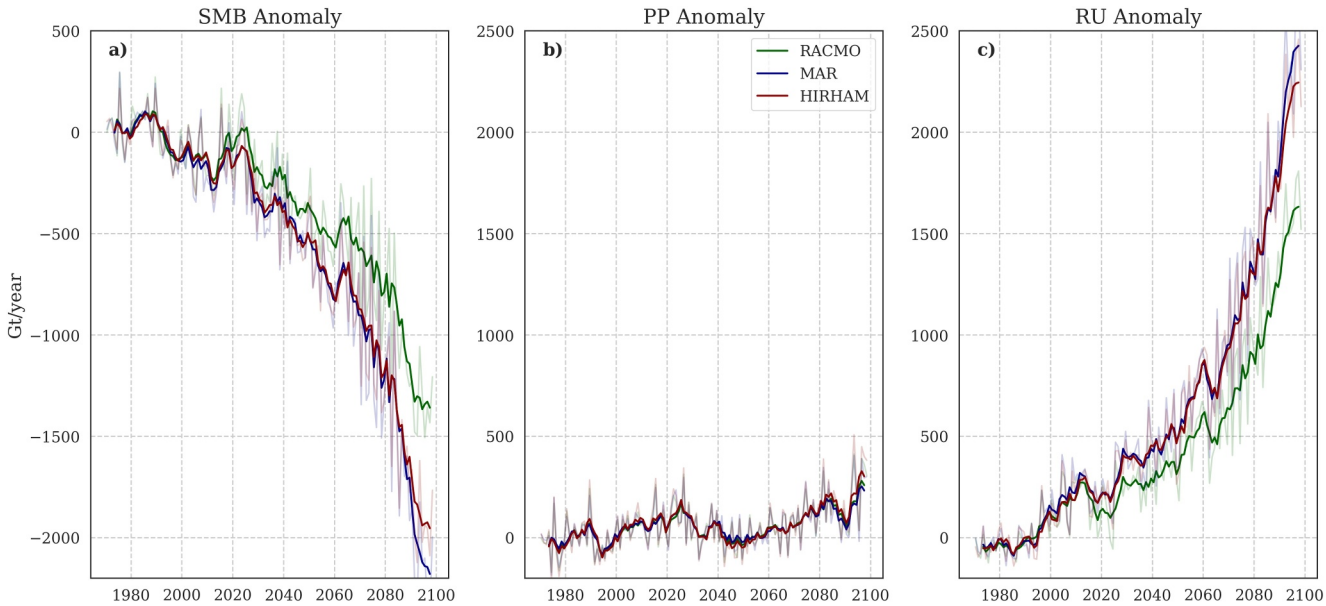

Figure 2. Spatially aggregated annual GrIS SMB anomalies (a), total precipitation (PP, b), and runoff (RU, c) [Gt/yr]. The solid lines represent the anomalies using a 5-year moving average, while the transparent lines display the unfiltered model output.

The increasing runoff following atmospheric warming (Figure 4c) strongly correlates with the increasing meltwater production (Figure 4a), with centered R^2 between these two variables of 0.98, 0.99, and 0.99 (RACMO, MAR, and HIRHAM, respectively). Comparing melt and subsequent runoff provides information on firn retention capacities at higher temperatures. While RACMO's firn model retains a significant portion of the meltwater within the snowpack (18% of firn refreezing and retention capacity at the end of the century), HIRHAM's firn model tends to convert more melt directly into runoff (only 6% of firn refreezing capacity).

Figure 5 summarizes the relationships between SMB, runoff, ablation zone fraction, and temperature anomalies for the RACMO, MAR, and HIRHAM models. As runoff increases, SMB decreases consistently ($R^2 > 0.95$),

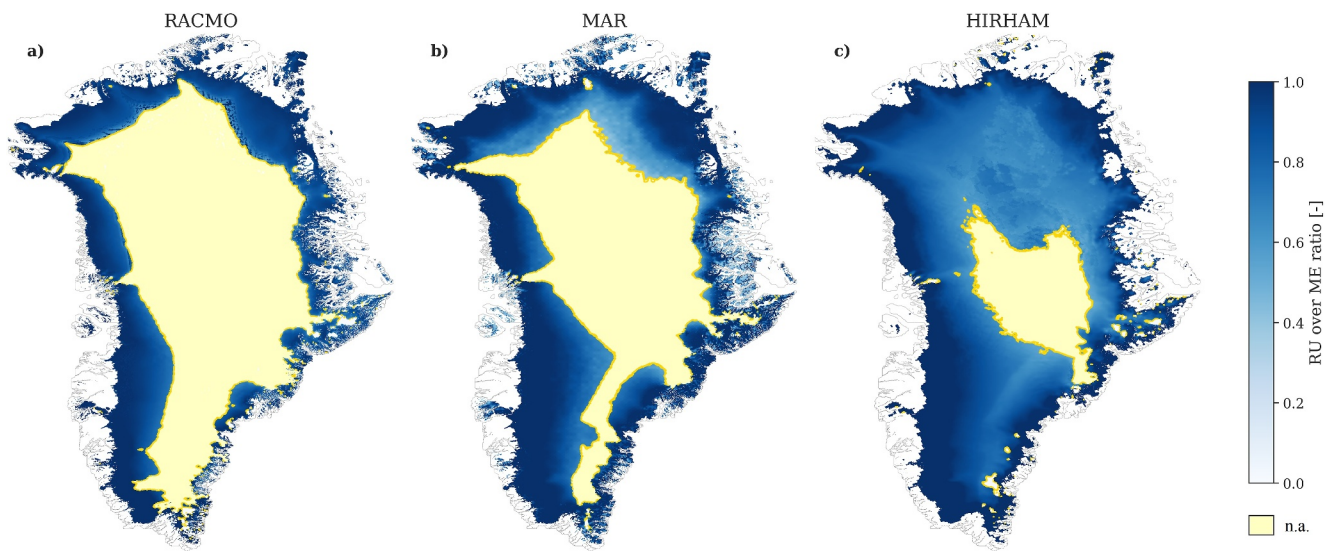

Figure 3. Fraction of meltwater running off from the GrIS by the end of the century (2080–2099), as modeled by (a) RACMO, (b) MAR, and (c) HIRHAM. The map extent is limited to the ablation zone (delimited by the equilibrium line, in yellow) considering the lower melt amount in the accumulation zone, and consequently noisy ratio values (numerical artifacts).

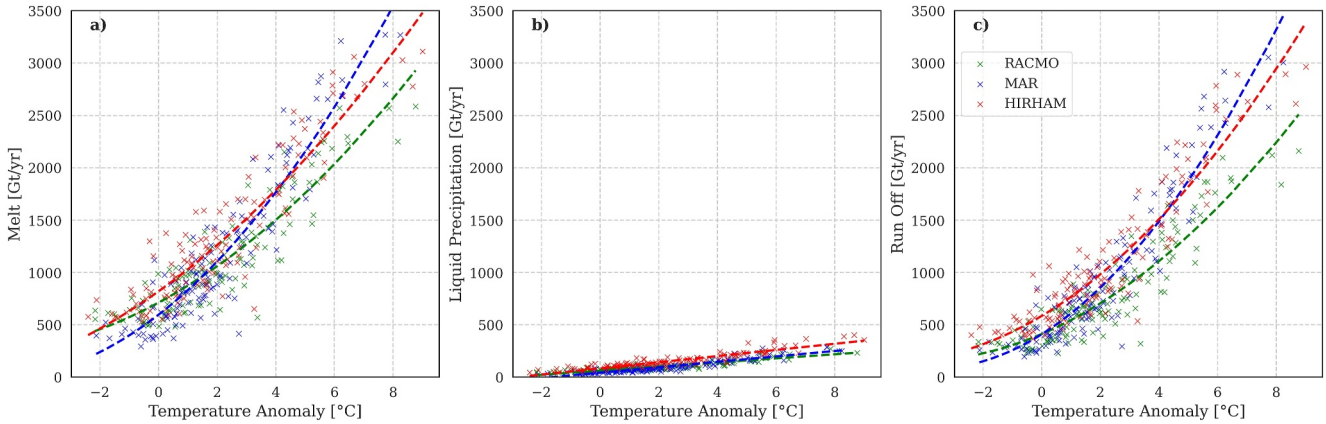

Figure 4. Melt (a), liquid precipitation (b), and runoff (c) sensitivity to 2-m temperature anomalies for RACMO, MAR, and HIRHAM. Each cross in the scatterplot represents one specific year for a given model (averaged RCM temperature anomaly, and summed *y*-axis value). Dashed lines represent first-order (b) and second-order polynomials (a and c).

following Equation 1 (Figure 5a). MAR and HIRHAM exhibit lower SMB values and higher runoff rates compared to RACMO, which shows a narrower range of SMB and runoff values.

As runoff increases, the ablation zone expands, expressed as a fraction of the total ice sheet area (Figure 5b). These results align with findings by Ryan et al. (2019) and Noël et al. (2019), highlighting the strong interconnection between ablation zone dynamics and runoff ($R^2 > 0.97$). The trend lines show different slopes for each model, indicating varying sensitivities. As shown in Figure 1, the ablation zone by the end of the century in RACMO is lower compared to MAR and HIRHAM (47% vs. 70% vs. 87%, respectively).

These results illustrate that the extent of the ablation zone is correlated with temperature anomalies (Figure 5c). As temperatures increase, runoff increases and the ablation zone expands, leading to a larger area deprived of firn, exposing dark baer ice at the surface. Lower albedo in the ablation zone triggers a positive melt-albedo feedback, thus enhancing surface runoff and further increasing the ablation zone extent. Increased temperatures also lead to more rainfall and melt over the current snowpack, depleting firn pore space and reducing retention, in turn enhancing runoff higher inland. Finally, given that mass gain from precipitation plays a secondary role on SMB change (Figure 2), enhanced surface runoff dominates the projected SMB decline.

4. Discussions

The primary source of the different GrIS SMB projections among RACMO, MAR, and HIRHAM, is the runoff component. The faster expansion of the ablation zone in MAR and HIRHAM (70% and 86% of the ice sheet area,

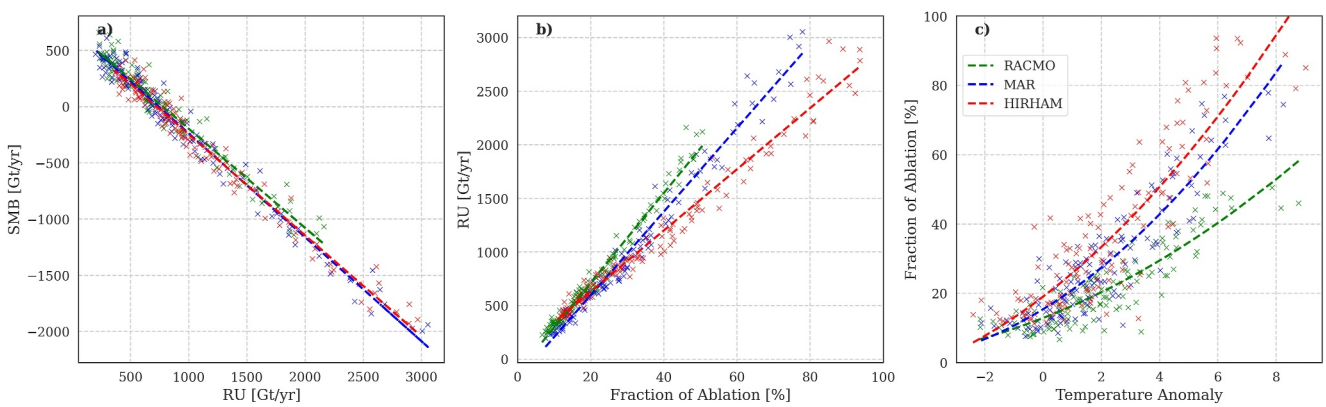

Figure 5. Relationships between Surface Mass Balance (SMB), runoff (RU), ablation zone extent (%), and temperature anomalies for the RACMO, MAR, and HIRHAM models. (a) Relationship between SMB and RU. (b) Relationship between RU and ablation zone extent (% of total GrIS area). (c) Expansion of the ablation zone extent with temperature anomalies. Each cross in the scatterplot represents 1 year for a model. Dashed lines represent trend lines.

respectively, over 2090–2099) compared to RACMO (47%) contributes to discrepancies in runoff projections. These discrepancies are influenced by the models' different sensitivities to atmospheric warming, affecting meltwater production and subsequent runoff. MAR and HIRHAM predict substantially higher meltwater production at increased temperature anomalies compared to RACMO, demonstrating a stronger non-linear response to warming. This higher sensitivity results in greater runoff in MAR and HIRHAM, amplifying the differences in SMB projections in the long run. In addition, the spatial distribution of mass loss varies between models (see Figure 1), which can have implications for the dynamic responses of the ice sheet, particularly if coupled with ice sheet models (Delhasse et al., 2024).

The presented numerical models, RACMO, MAR, and HIRHAM, each have their limitations, such as baer ice albedo prescription, firn model parameterization, and fixed ice sheet geometry. First, RACMO uses a fixed MODIS-based product for albedo over baer ice, whereas MAR and HIRHAM employ fixed predefined values. These albedo values can be quite different compared to observed albedo maps from satellite observations (Antwerpen et al., 2022), and are subject to future change as the baer ice area increases. Second, the different firn models used in the three climate models also impact runoff production, notably in the low percolation zone. As described in Section 2, the IWS threshold, that is, the maximum proportion of pore volume filled with water retained within the snowpack, varies among the models. MAR and HIRHAM have an IWS of 7%, while RACMO uses a value of 2%. In addition, the number of layers and the maximum depth of the numerical snowpack are different. All these parameters influence the retention of liquid water in the snowpack, affecting the amount of runoff. A higher IWS leads to increased runoff as it increases snow density, lowers albedo, increases melt and subsequently runoff (Brajkovic et al., 2023). Although a larger IWS provides more potential for refreezing, the resultant effects on the energy balance outweigh it. Third, the models' fixed ice sheet geometry has its limitations, including the exclusion of melt-elevation feedback, where increased surface temperature due to reduced surface height enhances melt, although this effect is limited over a one-century timescale. Addressing these limitations through model improvements and incorporating dynamic processes is essential for improving future projections.

5. Conclusions

This study highlights significant differences in SMB projections among three RCMs (RACMO, MAR, and HIRHAM) when forced by CESM2 under the high-end SSP5-8.5 scenario (−964, −1735, and −1698 Gt per year, respectively, for 2080–2099). The primary drivers of these discrepancies are differences in projected meltwater and associated runoff (1912, 2648, and 2651 Gt per year, respectively, for 2080–2099), influenced by varying sensitivities to atmospheric warming. Accurate SMB projections are crucial for understanding the GrIS contribution to global sea-level rise, and the differences identified underscore the need for improved model representations of meltwater production, refreezing processes, and surface albedo changes. This can be made possible by developing common frameworks for intercomparison exercises (Coupled Model Intercomparison Project - CMIP initiatives, such as Nowicki et al., 2016). This includes addressing parametric uncertainties, such as, but not limited to, the IWS threshold and albedo schemes. Coordinated efforts in future Ice Sheet Model Intercomparison Projects (e.g., ISMIP7) are essential to capture a range of potential future scenarios. Despite these differences, all models indicate a trend toward increased melt and runoff, suggesting a consistent direction in projected GrIS mass loss. By incorporating multiple RCMs in IPCC assessments and by including improved Greenland climate forcings, these projections can be made more robust and reliable, thus enhancing our understanding of the GrIS contribution to global sea-level rise.

Conflict of Interest

The authors declare no conflicts of interest relevant to this study.

Data Availability Statement

Major RCMs outputs are available in Zenodo via Glaude (2024).

References

Antwerpen, R. M., Tedesco, M., Fettweis, X., Alexander, P., & van de Berg, W. J. (2022). Assessing bare-ice albedo simulated by MAR over the Greenland ice sheet (2000–2021) and implications for meltwater production estimates. *The Cryosphere*, *16*(10), 4185–4199. https://doi.org/10.5194/tc-16-4185-2022

Acknowledgments
This project (PROTECT - Projecting Sea-Level Rise: from Ice Sheets to Local Implications) has received funding from the European Union's Horizon 2020 research and innovation programme under grant agreement 869304. This material reflects only the authors' view and the European Commission is not responsible for any use that may be made of the information it contains. Computational resources of MAR have been provided by the Consortium des Équipements de Calcul Intensif (CÉCI), funded by the Fonds de la Recherche Scientifique de Belgique (F.R.S.-FNRS) under Grant number 2.5020.11 and by the Walloon Region. Additional high-performance computing and storage resources were provided by Sigma2 - the National Infrastructure for High Performance Computing and Data Storage in Norway through projects NN8006 K, NN8085 K, NS5011 K, NS8006 K and NS8085 K. NH is supported by the Danish State through the National Centre for Climate Research (NCKF), and by the Novo Nordisk Foundation project PRECISE (NNF23OC0081251). HG has received funding from the Research Council of Norway under projects 270061, 295046 and 324639. Finally, the Netherlands Earth System Science Centre (NESSC) is acknowledged for their contribution.

Bevis, M., Harig, C., Khan, S. A., Brown, A., Simons, F. J., Willis, M., et al. (2019). Accelerating changes in ice mass within Greenland, and the ice sheet's sensitivity to atmospheric forcing. *Proceedings of the National Academy of Sciences*, *116*(6), 1934–1939. https://doi.org/10.1073/pnas.1806562116

Box, J. E., Hubbard, A., Bahr, D. B., Colgan, W. T., Fettweis, X., Mankoff, K. D., et al. (2022). Greenland ice sheet climate disequilibrium and committed sea-level rise. *Nature Climate Change*, *12*(9), 808–813. https://doi.org/10.1038/s41558-022-01441-2

Brajkovic, J., Delhasse, A., & Fettweis, X. (2023). Impact du contenu en eau sur la capacité de rétention simulée du manteau neigeux de la calotte du Groenland [Impact of water content on the simulated retention capacity of the Greenland ice sheet snowpack]. *Bulletin de la Société Géographique de Liège*, *80*(2023/1), 5–17. https://doi.org/10.25518/0770-7576.7061

Brun, E., David, P., Sudul, M., & Brunot, G. (1992). A numerical model to simulate snow-cover stratigraphy for operational avalanche forecasting. *Journal of Glaciology*, *38*(128), 13–22. https://doi.org/10.3189/S0022143000009552

Christensen, J. H., Carter, T. R., Rummukainen, M., Giorgi, F., Jones, R. G., Kolli, R. K., et al. (2007). Evaluating the performance and utility of regional climate models: The PRUDENCE project. *Climatic Change*, *81*(Suppl 1), 1–6. https://doi.org/10.1007/s10584-006-9211-6

Coléou, C., & Lesaffre, B. (1998). Irreducible water saturation in snow: Experimental results in a cold laboratory. *Annals of Glaciology*, *26*, 64–68. https://doi.org/10.3189/1998aog26-1-64-68

Danabasoglu, G., Lamarque, J.-F., Bacmeister, J., Bailey, D. A., DuVivier, A. K., Edwards, J., et al. (2020). The community Earth system model version 2 (CESM2). *Journal of Advances in Modeling Earth Systems*, *12*, e2019MS001916. https://doi.org/10.1029/2019MS001916

De Ridder, K., & Gallée, H. (1998). Land surface-induced regional climate change in southern Israel. *Journal of Applied Meteorology*, *37*(11), 1470–1485. https://doi.org/10.1175/1520-0450(1998)037<1470:lsircc>2.0.co;2

Eerola, K. (2006). *About the performance of the Hirlam version 7.0 (Tech. Rep. No. 51, Article 14)*. DMI.

Ettema, J., van den Broeke, M. R., van Meijgaard, E., & van de Berg, W. J. (2010). Climate of the Greenland ice sheet using a high-resolution climate model – Part 2: Near-surface climate and energy balance. *The Cryosphere*, *4*(4), 529–544. https://doi.org/10.5194/tc-4-529-2010

Fettweis, X., Hofer, S., Krebs-Kanzow, U., Amory, C., Aoki, T., Berends, C. J., et al. (2020). GrSMBMIP: Intercomparison of the modelled 1980-2012 surface mass balance over the Greenland Ice Sheet. *The Cryosphere*, *14*(11), 3935–3958. https://doi.org/10.5194/tc-14-3935-2020

Franco, B., Fettweis, X., Lang, C., & Erpicum, M. (2012). Impact of spatial resolution on the modelling of the Greenland ice sheet surface mass balance between 1990–2010, using the regional climate model MAR. *The Cryosphere*, *6*(3), 695–711. https://doi.org/10.5194/tc-6-695-2012

Gallee, H. (1995). Simulation of the mesocyclonic activity in the Ross sea, Antarctica. *Monthly Weather Review*, *123*(7), 2051–2069. https://doi.org/10.1175/1520-0493(1995)123<2051:sotmai>2.0.co;2

Gallée, H., & Schayes, G. (1994). Development of a three-dimensional meso-primitive equation model: Katabatic winds simulation in the area of Terra Nova Bay, Antarctica. *Monthly Weather Review*, *122*(4), 671–685. https://doi.org/10.1175/1520-0493(1994)122<0671:DOATDM>2.0.CO;2

Glaude, Q. (2024). A factor two difference in 21st-century Greenland ice sheet surface mass balance projections from three regional climate models for a strong warming scenario (SSP5-8.5) [Dataset]. *Zenodo*. https://doi.org/10.5281/zenodo.13270554

Goelzer, H., Nowicki, S., Payne, A., Larour, E., Seroussi, H., Lipscomb, W., et al. (2020). The future sea-level contribution of the Greenland ice sheet: A multi-model ensemble study of ISMIP6. *The Cryosphere*, *14*(9), 3071–3096. https://doi.org/10.5194/tc-14-3071-2020

Hanna, E., Cappelen, J., Fettweis, X., Mernild, S. H., Mote, T. L., Mottram, R., et al. (2021). Greenland surface air temperature changes from 1981 to 2019 and implications for ice-sheet melt and mass-balance change. *International Journal of Climatology*, *41*(S1), E1336–E1352. https://doi.org/10.1002/joc.6771

Hanna, E., Topál, D., Box, J. E., Buzzard, S., Christie, F. D. W., Hvidberg, C., et al. (2024). Short- and long-term variability of the Antarctic and Greenland ice sheets. *Nature Reviews Earth & Environment*, *5*(3), 193–210. https://doi.org/10.1038/s43017-023-00509-7

Hofer, S., Lang, C., Amory, C., Kittel, C., Delhasse, A., Tedstone, A., & Fettweis, X. (2020). Greater Greenland Ice Sheet contribution to global sea level rise in CMIP6. *Nature Communications*, *11*(1), 6289. https://doi.org/10.1038/s41467-020-20011-8

Howat, I. M., Negrete, A., & Smith, B. E. (2014). The Greenland Ice Mapping Project (GIMP) land classification and surface elevation data sets. *The Cryosphere*, *8*(4), 1509–1518. https://doi.org/10.5194/tc-8-1509-2014

IMBIE. (2019). Mass balance of the Greenland ice sheet from 1992 to 2018. *Nature*, *579*(7798), 233–239. https://doi.org/10.1038/s41586-019-1855-2

IPCC. (2023). In H. Lee, & J. Romero (Ed.), *Climate Change 2023: Synthesis report. Contribution of Working Groups I, II, and III to the Sixth Assessment Report of the Intergovernmental Panel on Climate Change*. IPCC. https://doi.org/10.59327/IPCC/AR6-9789291691647

Kuipers Munneke, P., van den Broeke, M. R., Lenaerts, J. T. M., Flanner, M. G., Gardner, A. S., & van de Berg, W. J. (2011). A new albedo parameterization for use in climate models over the Antarctic ice sheet. *Journal of Geophysical Research*, *116*(D5), D05114. https://doi.org/10.1029/2010JD015113

Lambin, C., Fettweis, X., Kittel, C., Fonder, M., & Ernst, D. (2023). Assessment of future wind speed and wind power changes over South Greenland using the Modèle Atmosphérique Régional regional climate model. *International Journal of Climatology*, *43*(1), 558–574. https://doi.org/10.1002/joc.7795

Langen, P. L., Mottram, R. H., Christensen, J. H., Boberg, F., Rodehacke, C. B., Stendel, M., et al. (2015). Quantifying energy and mass fluxes controlling Godthåbsfjord freshwater input in a 5-km simulation (1991–2012). *Journal of Climate*, *28*(9), 3694–3713. https://doi.org/10.1175/JCLI-D-14-00271.1

Lefebre, F., Fettweis, X., Gallée, H., Van Ypersele, J.-P., Marbaix, P., Greuell, W., & Calanca, P. (2005). Evaluation of a high-resolution regional climate simulation over Greenland. *Climate Dynamics*, *25*(1), 99–116. https://doi.org/10.1007/s00382-005-0005-8

Ligtenberg, S. R. M., Helsen, M. M., & van den Broeke, M. R. (2011). An improved semi-empirical model for the densification of Antarctic firn. *The Cryosphere*, *5*(4), 809–819. https://doi.org/10.5194/tc-5-809-2011

Morcrette, J.-J. (2002). Assessment of the ECMWF model cloudiness and surface radiation fields at the ARM SGP site. *Monthly Weather Review*, *130*(2), 257–277. https://doi.org/10.1175/1520-0493(2002)130

Morlighem, M., Williams, C. N., Rignot, E., An, L., Arndt, J. E., Bamber, J. L., et al. (2017). BedMachine v3: Complete bed topography and ocean bathymetry mapping of Greenland from multibeam echo sounding combined with mass conservation. *Geophysical Research Letters*, *44*(21), 11051–11061. https://doi.org/10.1002/2017GL074954

Mottram, R., Boberg, F., Langen, P., Yang, S., Rodehacke, C., Christensen, J. H., & Madsen, M. S. (2017). Surface mass balance of the Greenland ice sheet in the regional climate model HIRHAM5: Present state and future prospects. 低温科学, *75*, 105–115. http://hdl.handle.net/2115/65106

Noël, B., Lenaerts, J. T. M., Lipscomb, W. H., Thayer-Calder, K., & van den Broeke, M. R. (2022). Peak refreezing in the Greenland firn layer under future warming scenarios. *Nature Communications*, *13*(1), 6870. https://doi.org/10.1038/s41467-022-34524-x

Noël, B., van de Berg, W. J., Lhermitte, S., & van den Broeke, M. R. (2019). Rapid ablation zone expansion amplifies north Greenland mass loss. *Science Advances*, *5*(9), eaaw0123. https://doi.org/10.1126/sciadv.aaw0123

Noël, B., van de Berg, W. J., Machguth, H., Lhermitte, S., Howat, I., Fettweis, X., & van den Broeke, M. R. (2016). A daily, 1 km resolution data set of downscaled Greenland ice sheet surface mass balance (1958–2015). *The Cryosphere*, *10*(5), 2361–2377. https://doi.org/10.5194/tc-10-2361-2016

Noël, B., van Kampenhout, L., Lenaerts, J. T. M., van de Berg, W. J., & van den Broeke, M. R. (2021). A 21st century warming threshold for sustained Greenland ice sheet mass loss. *Geophysical Research Letters*, *48*(5), e2020GL090471. https://doi.org/10.1029/2020GL090471

Noël, B., van Kampenhout, L., van de Berg, W. J., Lenaerts, J. T. M., Wouters, B., & van den Broeke, M. R. (2020). Brief communication: CESM2 climate forcing (1950–2014) yields realistic Greenland ice sheet surface mass balance. *The Cryosphere*, *14*(4), 1425–1435. https://doi.org/10.5194/tc-14-1425-2020

Nowicki, S. M. J., Payne, A., Larour, E., Seroussi, H., Goelzer, H., Lipscomb, W., et al. (2016). Ice sheet model intercomparison project (ISMIP6) contribution to CMIP6. *Geoscientific Model Development*, *9*(12), 4521–4545. https://doi.org/10.5194/gmd-9-4521-2016

Oerlemans, J., & Knap, W. H. (1998). A 1 year record of global radiation and albedo in the ablation zone of Morteratschgletscher, Switzerland. *Journal of Glaciology*, *44*(147), 231–238. https://doi.org/10.3189/S0022143000002574

Porter, C., Morin, P., Howat, I., Noh, M.-J., Bates, B., Peterman, K., et al. (2018). ArcticDEM, version 3 (V1). *Harvard Dataverse*. https://doi.org/10.7910/DVN/OHHUKH

Roeckner, E., Bäuml, G., Bonaventura, L., Brokopf, R., Esch, M., Giorgetta, M., et al. (2003). The atmospheric general circulation model ECHAM 5. PART I: Model description (max Planck Institute for meteorology report No. 349).

Ryan, J. C., Smith, L. C., van As, D., Cooley, S. W., Cooper, M. G., Pitcher, L. H., & Hubbard, A. (2019). Greenland Ice Sheet surface melt amplified by snowline migration and bare ice exposure. *Science Advances*, *5*(3), eaav3738. https://doi.org/10.1126/sciadv.aav3738

Tedesco, M., & Fettweis, X. (2020). Unprecedented atmospheric conditions (1948–2019) drive the 2019 exceptional melting season over the Greenland ice sheet. *The Cryosphere*, *14*(4), 1209–1223. https://doi.org/10.5194/tc-14-1209-2020

Tedesco, M., Fettweis, X., Mote, T., Wahr, J., Alexander, P., Box, J. E., & Wouters, B. (2013). Evidence and analysis of 2012 Greenland records from spaceborne observations, a regional climate model and reanalysis data. *The Cryosphere*, *7*(2), 615–630. https://doi.org/10.5194/tc-7-615-2013

van Kampenhout, L., Lenaerts, J. T. M., Lipscomb, W. H., Lhermitte, S., Noël, B., Vizcaíno, M., et al. (2020). Present-day Greenland ice sheet climate and surface mass balance in CESM2. *Journal of Geophysical Research: Earth Surface*, *125*(2), e2019JF005318. https://doi.org/10.1029/2019JF005318

References From the Supporting Information

Langen, P. L., Fausto, R. S., Vandecrux, B., Mottram, R. H., & Box, J. E. (2017). Liquid water flow and retention on the Greenland ice sheet in the regional climate model HIRHAM5: Local and large-scale impacts. *Frontiers in Earth Science*, *4*. https://doi.org/10.3389/feart.2016.00110